Long-term clinical study and multiscale analysis of in vivo biodegradation mechanism of Mg alloy

Jee-Wook Lee[a,1], Hyung-Seop Han[b,1], Kyeong-Jin Han[c,1], Jimin Park[b], Hojeong Jeon[b,d], Myoung-Ryul Ok[b], Hyun-Kwang Seok[b,d], Jae-Pyoung Ahn[e], Kyung Eun Lee[e], Dong-Ho Lee[f], Seok-Jo Yang[g], Sung-Youn Cho[h], Pil-Ryung Cha[a], Hoon Kwon[a], Tae-Hyun Nam[i], Jee Hye Lo Han[h], Hyoung-Jin Rho[b], Kang-Sik Lee[f,2], Yu-Chan Kim[b,d,2], and Diego Mantovani[j]

[a]School of Advanced Materials Engineering, Kookmin University, Seoul 136-702, South Korea; [b]Center for Biomaterials, Korea Institute of Science & Technology, Seoul 136-650, South Korea; [c]Department of Orthopaedic Surgery, Ajou University School of Medicine, Suwon 443-721, South Korea; [d]Department of Bio-medical Engineering, University of Science & Technology, Daejeon 305-350, South Korea; [e]Advanced Analysis Center, Korea Institute of Science & Technology, Seoul 136-650, South Korea; [f]Department of Orthopaedic Surgery, Asan Medical Center, University of Ulsan College of Medicine, Seoul 138-736, South Korea; [g]Department of Mechatronics Engineering, Chungnam National University, Daejeon 305-764, South Korea; [h]R&D Center, U & I Corporation, Uijongbu 480-050, South Korea; [i]School of Nano and Advanced Materials Engineering, Gyeongsang National University, Jinju 660-701, South Korea; and [j]Laboratory for Biomaterials and Bioengineering, Department of Mining, Laval University, Québec City, QC, Canada G1V 0A6

Edited by John T. Potts, Massachusetts General Hospital, Charlestown, MA, and approved December 7, 2015 (received for review September 14, 2015)

There has been a tremendous amount of research in the past decade to optimize the mechanical properties and degradation behavior of the biodegradable Mg alloy for orthopedic implant. Despite the feasibility of degrading implant, the lack of fundamental understanding about biocompatibility and underlying bone formation mechanism is currently limiting the use in clinical applications. Herein, we report the result of long-term clinical study and systematic investigation of bone formation mechanism of the biodegradable Mg-5wt%Ca-1wt%Zn alloy implant through simultaneous observation of changes in element composition and crystallinity within degrading interface at hierarchical levels. Controlled degradation of Mg-5wt%Ca-1wt%Zn alloy results in the formation of biomimicking calcification matrix at the degrading interface to initiate the bone formation process. This process facilitates early bone healing and allows the complete replacement of biodegradable Mg implant by the new bone within 1 y of implantation, as demonstrated in 53 cases of successful long-term clinical study.

biodegradable implant | bone formation | clinical application

The century-old concept of the fixation device that holds the fractured bones in place to allow repair through the natural bone remodeling process is still being practiced today without alteration (1–5). The recent rapid growth of the elderly demographic of physically active adults has tremendously intensified the occurrence of bone trauma cases, highlighting once again the major drawbacks of current surgical approaches and osteosynthesis systems, such as inevitable secondary surgery to remove the inert fixation devices after complete bone healing and inflammatory response due to the release of metal ions. In the past decade, countless studies have been performed to control and optimize the mechanical and corrosion properties of magnesium-based alloys (6–9), which, thanks to their degradation in the physiological environment, could overcome the limitations of inert implant materials and shift the paradigm of conventional bone fixation devices toward new horizons. Driven by these new possibilities, important findings regarding, among others, the degradation mechanism of Mg-based alloys (10, 11), the formation of corrosion protective layers by degradation products (12, 13), and the osteogenetic properties of Mg ions (14, 15) have been reported in the literature. However, such findings are based on the observation of degradation products and of bone healing at the macroscale level. Due to lack of fundamental understanding on biocompatibility and underlying bone formation mechanism of the degradation product, there is so far only one known case of statistically insignificant clinical study result (16) with a short-term follow-up. In our previous study, we reported successful development and long-term in vivo study of uniformly slowly degrading Mg-5wt%Ca-1wt%Zn alloy system (*SI Appendix*, Figs. S1 and S2) featuring adequate mechanical strength [ultimate tensile strength (UTS) ~250 MPa] (17) and containing Ca, known to stimulate the formation of bone, and Zn, known to influence the remodeling of bone (18).

Herein, results from open-label interventional long-term clinical study of biodegradable Mg-5wt%Ca-1wt%Zn alloy screws for hand and wrist fractures are reported to demonstrate the clinical efficacy, safety, and feasibility. Furthermore, to identify the fundamental mechanisms by which Mg-5wt%Ca-1wt%Zn alloys promote new bone formation at multiscale levels of the same region, we combined Villanueva staining technique with nanoanalytical imaging methods based on SEM and transmission electron microscopy (TEM). Particularly, cover glass-free tissue slides were prepared to permit the observation of exactly the same region from macro- to micro- to nanoscale using three different analytical microscopes allowing the complete and thorough analysis of the Mg alloy–bone interface from a metallographic perspective. Such an approach allowed, to our knowledge for the first time, to systematically investigate the bone formation and to

Significance

In the past decade, countless studies have been performed to control the mechanical and corrosion property of magnesium-based alloy, which degrades in the physiological environment, to overcome the flaws of the inert implant materials and shift the paradigm of conventional bone fixation devices. Controlled degradation of Mg-5wt%Ca-1wt%Zn alloy results in the formation of biomimicking calcification matrix at the degrading interface to initiate the bone formation process. This process facilitates early bone healing and allows the complete replacement of biodegradable Mg implant by the new bone within 1 y of implantation, as demonstrated in 53 cases of successful long-term clinical study.

Author contributions: J.-W.L., H.-S.H., H.-K.S., K.-S.L., and Y.-C.K. designed research; J.-W.L., H.-S.H., K.-J.H., J.P., H.J., M.-R.O., J.-P.A., D.-H.L., S.-J.Y., S.-Y.C., P.-R.C., H.K., T.-H.N., J.H.L.H., H.-J.R., K.-S.L., and Y.-C.K. performed research; S.-J.Y. and D.M. contributed new reagents/analytic tools; J.P., H.J., J.-P.A., K.E.L., P.-R.C., and D.M. analyzed data; K.-J.H. performed clinical trial; and J.-W.L., H.-S.H., and Y.-C.K. wrote the paper.

The authors declare no conflict of interest.

This article is a PNAS Direct Submission.

Freely available online through the PNAS open access option.

[1]J.-W.L., H.-S.H., and K.-J.H. contributed equally to this work.

[2]To whom correspondence may be addressed. Email: chany@kist.re.kr or klee@amc.seoul.kr.

This article contains supporting information online at www.pnas.org/lookup/suppl/doi:10.1073/pnas.1518238113/-/DCSupplemental.

www.pnas.org/cgi/doi/10.1073/pnas.1518238113

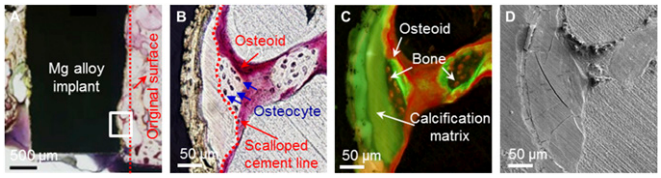

Fig. 1. Histological and SEM analysis of rabbit femoral condyle after 8 wk of implantation of Ø 2 × 6-mm cylindrical Mg alloy implant. (*A*) Implant–bone interface at low magnification, the degradation of the Mg alloy implant is evidenced by drawing the original surface line. Magnified image of bone formation region observed by (*B*) light microscopy, (*C*) fluorescence microscopy, and (*D*) SEM.

monitor the changes occurring at of the interface between Mg alloy and bone by analyzing element composition and crystallinity using histology, TEM, and SEM.

Results

Hierarchical Multiscale Analysis of the Implant–Bone Interface. Villanueva staining is a histological technique for undecalcified tissue and allows the observation of highly reactive Mg alloy interface without the occurrence of additional corrosion reactions caused by the staining agents itself. The examination of the distinguishable acellular bone matrix, which is nearly impossible through conventional histological method using optical microscopy (19), could be performed using Villanueva stain and fluorescence microscopy (*SI Appendix*, Fig. S3). Along with typical histomorphometric evaluation, by s.c. administering calcein (CA) as a fluorescent dye, it was possible to clearly distinguish the location of newly formed bone from previously existing bones (20). Fig. 1*A* shows the interface of Mg alloy at 8 wk postimplantation, and an area where new bone formation was observed was farther investigated at higher magnifications by both light and fluorescence microscopy (Fig. 1 *B* and *C*). Observation of these regions revealed a close relationship between the new bone formation and calcified matrix consisting of calcium phosphates and Mg alloy degradation products (21). Bone formation activities of osteoblasts (OB) following the resorption of osteoclasts (OC) were evident in the calcified matrix on the interface, which is in contact with the bone and scalloped cement line (Fig. 1*B*) (22, 23). These new bone formation lines suggest favorable bone formation by the Mg-degradation by-products, further supported by the in-depth analysis at micro and nano levels using SEM (Fig. 1*D* and 2*A*) and TEM (Fig. 2 *B* and *C*).

SEM and TEM Analysis of the Implant–Bone Interface. To investigate the chemical changes in the newly generated tissues during the Mg alloy degradation process, five different regions at increasing distance from the implant were identified based on chemical composition changes from the merged image of the fluorescence and SEM images as shown on Fig. 2*A*, *i*, and energy-dispersive X-ray spectroscopy (EDX) analysis were performed (Fig. 2*A*, *ii*). Region I, which is located right next to Mg alloy, contained a lot more Mg and O than Ca and P. As previously reported in various in vitro biocorrosion studies, this region was identified as the well-known degradation by-product, $Mg(OH)_2$ layer (10, 11). Relative intensities of Mg, O, Ca, and P peaks were quantitatively measured from the implant surface to the 220-μm distance from the surface using EDX analysis. We found that the relative peak intensities of Mg and O decreased along the distance from the implant surface. Mg peaks were sharply decreased ∼30 μm from the implant surface, and no Mg peaks were observed ∼150 μm from the implant surface. O peaks gradually decreased from the implant surface without an apparent sharp decrease. However, Ca and P peaks increased along the distance, and both peaks showed drastic increase ∼30 μm from the implant surface. Additionally, both peak intensities remained constant to 120 μm from the implant surface, and intensities again decreased to

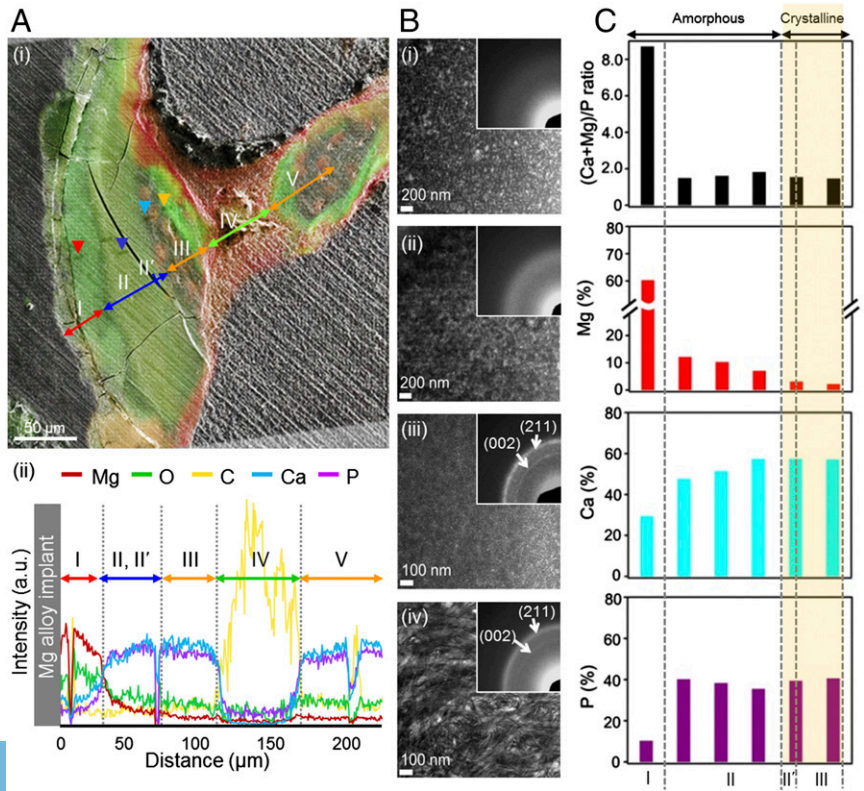

Fig. 2. Hierarchical multiscale analysis of Mg alloy–implant interface. (*A*) Separation of regions in Mg alloy–implant interface: (*i*) merged image of the fluorescence and SEM images and (*ii*) SEM/EDX line profile. (*B*) Changes in the microstructure of the key regions; TEM images and SAD pattern (*Inset*) of (*i*) region I (Mg, O-rich: red arrowhead of *A*, *i*), (*ii*) region II (Ca, P-rich: blue arrowhead), (*iii*) region II′ (Ca, P-rich: sky-blue arrowhead), (*iv*) region III (bone: orange arrowhead). (*C*) TEM/EDX change of (Mg + Ca)/P ratio, Mg (%), Ca (%), and P (%) throughout regions I, II, II′, and III.

nearly zero ~150 μm from the surface. Such increase of Ca and P in region II indicated deposition of calcification matrix in place of the degradation product, and it is distinguishable by the difference in green color contrast of the region I. Region III shows a bone area having similar elemental composition to region II but a different green fluorescence signal, possibly related to a change of the crystallinity of calcium phosphates, which will be discussed in detail in the latter part of this manuscript. Red-colored osteoid region (region IV) does not contain Ca or P, indicating a lack of mineralization (24). Results from fluorescent histology, images from SEM, and distribution of composition from EDX mapping (*SI Appendix*, Fig. S4) clearly showed that region V is identical to the bone area in region III.

Focusing on the three regions that showed large compositional differences as observed by SEM and histology, four specific points (arrowheads on Fig. 2*A*, *i*) were selected, and microstructural crystallographic characterizations were performed using TEM. As shown in Fig. 2*B*, selected points included Mg and O-rich area from region I, center of Ca, P-rich area from region II, Ca, P-rich area from scalloped cement line within region II (region II′), and bone area from region III.

Region I (Fig. 2*B*, *i*) had an amorphous structure with a broad ring pattern observed by selected area diffraction (SAD), which indicates the accumulation of amorphous Mg and O-rich compound at the surface of Mg alloy, where degradation occurs by electrochemical reaction (*SI Appendix*, Fig. S5). Interestingly, region II also showed an amorphous ring pattern (Fig. 2*B*, *ii*) whereas region II′ (Fig. 2*B*, *iii*) consisted of crystalline calcium phosphate phase with clear observation of (002) and (211) planes (*SI Appendix*, Fig. S6). In addition, region III (Fig. 2*B*, *iv*) had typical bone-like microstructure, and observation of SAD pattern revealed (002) and (211) planes, which has bone-specific c-axis orientation. The most intriguing information obtained from the structural observation through TEM is found within region II′, which indicates crystallization of Ca, P-rich phase before development of mature bone tissue. The presence of a scalloped cement line in the vicinity of the Ca, P-rich region II′, with a crystalline structure similar to the bone, suggests proper bone formation initiated by recruitment of OC that recognized region II′ as natural bone.

Bone Formation During Biodegradation of Mg Alloy Implant. Biodegradation of Mg alloy implant occurs continuously throughout the implantation period (*SI Appendix*, Fig. S7), and the vacant degradation site is occupied by a calcified matrix that is later resorbed and substituted by new bone (Fig. 3 and *SI Appendix*, Fig. S8). In general, biodegradation of Mg alloy implant occurs throughout the implantation period and the volume is gradually reduced as time progress from 8 to 26 wk (*SI Appendix*, Fig. S7). The above-mentioned Mg alloy–bone interface also shifts to the implant center as implantation time is prolonged, and ~15% shift was observed from the original surface line after every 8 wk of implantation period. At 16 wk, ~30% shift was made, and ~45% shift was observed after 24 wk (Fig. 3). As shown in *SI Appendix*, Fig. S8, degraded volume and shifting Mg–bone interface is followed by the formation of calcification matrix, resorption of calcification matrix by the OC, and bone formation by OB, and gets replaced with degradation products and new bone. The apparent wave-like progress of the implant degradation surface is due to the difference in speed of simultaneously occurring bone remodeling cycle, which depends on the location of the bone. Throughout the entire degradation process, simultaneous repetitive reactions and biological processes allow the Mg alloy implant to degrade and consistently structure interface layers where new bone deposition is performed. Thus, regions I–V shown in Fig. 2*A* are always observed during such process. The above-mentioned bone formation aiding mechanism of Mg alloy degradation led to series of positive results from the in vivo studies, and bone formation aiding ability of Mg alloy can be compared with the conventional titanium implant, as shown in *SI Appendix*, Fig. S9.

Long-Term Clinical Observation. Fundamental findings of this study and the successful outcome of 53 clinical trial cases performed at Ajou University Hospital (Suwon, Korea) provide solid scientific rationale and demonstrate the endless possibility of biodegradable implant devices. Fig. 4 shows the radiographic images of selected 1-y follow-up of the 29-y-old female patient. Surgical fixation of distal radius was performed with Mg-5wt%Ca-1wt%Zn screw (*SI Appendix*, Fig. S10), and two conventional stainless steel pins were used to fix the scaphoid fracture (Fig. 4*B*, *i* and *ii*). After 6 mo of surgical fixation (Fig. 4*B*, *iii*), the distal radius fracture is completely healed with a small radiolucent area in the

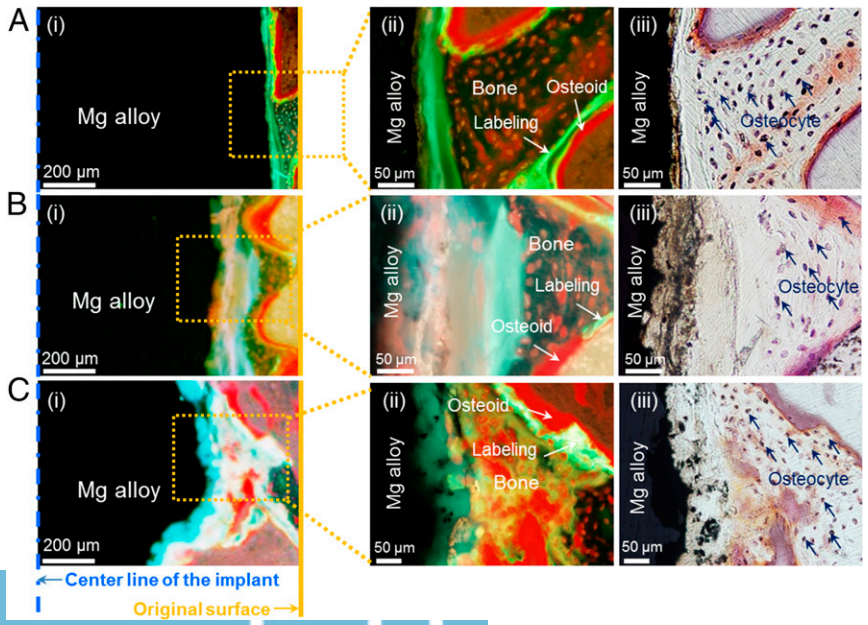

Fig. 3. Gradual degradation of the Mg alloy interface and bone formation stained with Villanueva stain method at (*A*) 8 wk, (*B*) 16 wk, and (*C*) 26 wk postimplantation. (*A*, *i*) Mg alloy degradation observed under fluorescence light in low magnification at 8 wk, (*B*, *i*) 16 wk, and (*C*, *i*) 26 wk postimplantation. (*A*, *ii*) Bone formation observed in fluorescence light at high magnification at 8 wk, (*B*, *ii*) 16 wk, and (*C*, *ii*) 26 wk postimplantation. (*A*, *iii*) Bone formation observed in natural light at high magnification of 8 wk, (*B*, *iii*) 16 wk, and (*C*, *iii*) 26 wk postimplantation. Straight line in *A*, *i*, *B*, *i*, and *C*, *i*, indicates original implant surface line; dotted line refers to the center of implants at the time of implantation.

Table 1. Follow-up data of 53 clinical cases

Category	Follow-up, mo		
	12	6	3
Cases (male/female)	28 (22/6)	15 (10/5)	10 (9/1)
Bone union/nonunion	28/0	15/0	10 /0
VAS*		1.38 ± 1.1	
DASH†		29.82 ± 4.4	

Case was considered distinct if same patient received screw in different location.
*Visual analog scales ranging from 0 (no pain) to 10 (worst possible pain).
†Disabilities of the arm, shoulder, and hand ranging from 0 (no disability) to 100 (extreme disability).

screw insertion site. The cortical continuity is observed and the diameter of the inserted Mg alloy screw was significantly reduced. The patient did not feel any discomfort or pain throughout the entire study. At 1 y postoperation (Fig. 4*B*, *iv*), the distal radius fracture is completely healed and it is nearly impossible to differentiate the remaining Mg alloy screw from new surrounding bones. A 3D schematic provides a clear overview of the case (Fig. 4*C*), and similar positive results were observed for all other clinical cases without a single failure (*SI Appendix*, Figs. S11 and S12). After 12 and 6 mo of implantation, patients involved in 53 cases of clinical trials initiated in July 2013 returned to their everyday life and career without any sign of pain, and pain level according to the Visual Analog Scale was ~1.38 ± 1.1 (Table 1). Patients did not show decrease in range of motion, and gained back normal range of grip power. The disabilities of the arm, shoulder and hand (DASH) was measured to be 29.82 ± 4.4 at 6 mo. All patients involved in the clinical study showed normal healing rate without any sign of pain.

Discussion

Detailed formation pathways of three regions (I, II, and II′) from the degrading interface can be considered as follows. At first, corrosion of Mg alloy surface enables a series of reactions within the physiological environment leading to the formation of the amorphous Mg and O-rich compound, $Mg(OH)_2$, as supported by the elemental analysis of region I. Indeed, previous reports observed similar formation of $Mg(OH)_2$ precipitates around the degrading Mg surfaces (25, 26). With the experimental evidences, Mg-Ca-Zn alloy degradation and formation of by-product can be described from the thermodynamic point of view. Considering that our alloy is mainly composed of Mg, the dominant anodic reaction by the degradation of our alloy in aqueous solution at pH of ~7.4 can be represented as follows:

$$Mg + 2H_2O \leftrightarrow Mg^{2+} + 2OH^- + H_2\uparrow \quad [1]$$

Formation of hydroxyl ions resulting from reaction of Eq. **1** increases the local pH at the initial degrading interface of Mg alloy. Simultaneous increase in pH and Mg ion concentration will reach a critical point, moving the solubility equilibrium of Mg toward the production of precipitated $Mg(OH)_2$ (21).

$$Mg(OH)_2 \leftrightarrow Mg^{2+} + 2OH^- \quad [2]$$

The equilibrium constant, K_{sp} for the above reaction is $[Mg^{2+}][OH^-]^2 = 8.9 \times 10^{-12}$ (27). Reverse reaction from Eq. **2** would cause precipitation of $Mg(OH)_2$ if the $[Mg^{2+}][OH^-]^2$ value by pH and Mg ion concentration increased by the Eq. **1** reaction exceeds the above K_{sp}. In other words, degrading interface of Mg alloy implanted in physiological environment experiences increase of pH and Mg ion concentration from reaction shown in Eq. **1**, finally leading to the deposition of $Mg(OH)_2$. In this light and based on the results of EDX elemental profiles (Fig. 2*A*, *ii*), region

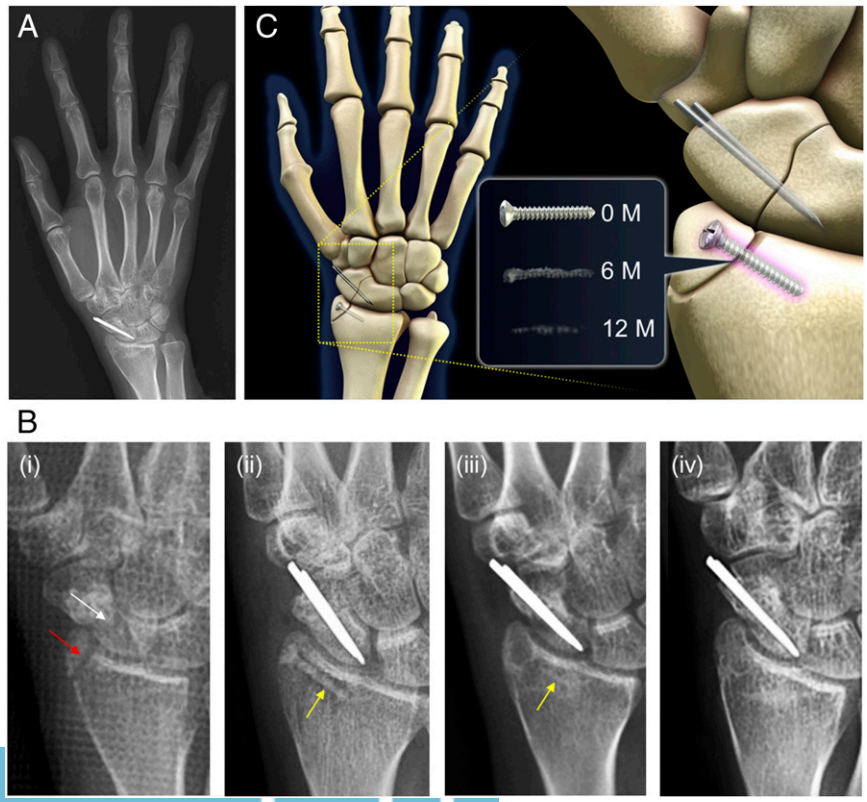

Fig. 4. Clinical observation of complete degradation and bone healing of Mg alloy screw over a 1-y period. (*A*) A 1-y follow-up X-ray of patient that received Mg alloy implant (D 2.3 mm × L 14 mm) for the distal radius fracture and stainless steel conventional implant (CI) for the scaphoid nonunion. (*B*) X-ray images of (*i*) the distal radius fracture and the scaphoid nonunion before the surgical intervention, (*ii*) implantation site immediately taken after the surgical procedures to fix the distal radius fracture with Mg alloy implant and the scaphoid nonunion with CI, (*iii*) 6-mo follow-up, and (*iv*) complete degradation and bone healing after 1 y postoperation. (*C*) Schematic diagram showing implantation site and the change of Mg alloy over time: immediately, 6 mo, and 1 y after implantation. Red arrow shows the distal radius fracture, and white arrow is pointing at the scaphoid nonunion. Yellow arrow shows the Mg alloy implant.

I shown in Fig. 2 can be expected as the interface area occupied by freshly deposited $Mg(OH)_2$ produced by the degradation of the Mg alloy.

This increase in pH near the local degrading surfaces can trigger another competitive reaction, precipitation of calcium phosphate compounds. The reaction for hydroxyapatite (HA) formation, one of the major calcium phosphate compounds in human body, can be described as follows:

$$5Ca^{2+} + 3PO_4^{3-} + OH^- \leftrightarrow Ca_5(PO_4)_3(OH) \quad [3]$$

Equilibrium constant K_{sp} for hydroxyapatite is equal to $[Ca^{2+}]^5[PO_4^{3-}]^3[OH^-] = 2.2 \times 10^{-61}$ (28). Similar with the $Mg(OH)_2$, as pH increases, the thermodynamic driving force leading to formation of solid precipitates increases as well. However, it should be noted that increase in Mg^{2+} did not promote the formation of hydroxyapatite, contrary to the case of $Mg(OH)_2$. According to the results from TEM/EDX analysis (Fig. 2*C*), Mg from Mg + Ca + P fraction clearly decreased due to the diffusing process as one move away from the Mg implant surface toward the native bone. In contrast, Ca showed an opposite trend and increased as the Mg decreased. In this regard, we believed that higher Mg ion concentration in region I results in dominant formation of $Mg(OH)_2$ phase, whereas calcium phosphate formation becomes the more dominant pathway in lower Mg ion concentration region, region II and II′.

It is intriguing that region II is comprised of amorphous calcification matrix, considering that crystalline calcium phosphate is a more thermodynamically stable phase than its amorphous counterpart. The reason for the first appearance of amorphous calcium phosphate (ACP) before crystalline one can be hypothesized as follows. First, because the amorphous structure is more similar to that of liquid solution, the kinetic energy barrier for the formation of amorphous structured ACP is expected to be lower than that of crystalline HA, and, consequently, ACP can be formed before HA. Preferential formation of thermodynamically metastable phase, followed by transformation to thermodynamically stable phase due to lower energy barrier, is well known as the Ostwald step rule (29). Moreover, previous reports showed that Mg ion can effectively stabilize ACP by adsorbing onto the ACP, and this stabilization retards phase transformation of ACP into HA. All of these explanations might cause preferential formation of amorphous ACP, which in turn transforms to thermodynamically more stable crystalline HA. After maturation, microcrystal of crystallized calcium phosphates (CCPs) are known to form from ACPs (30, 31), leading to the appearance of newly formed crystalline regions such as region II′ observed in Fig. 2. CCP in region II′ (Fig. 2*B*, *iii*) exhibits low Mg content, similar to that of native bone region.

It is noteworthy that physiological homeostasis processes locally lower high pH values to the normal pH range, cyclically fostering the formation of ACP from $Mg(OH)_2$ and the degradation of Mg, according to Eqs. **1** and **2**. Throughout the entire degradation process, these simultaneous repetitive reactions allow the Mg alloy implant to degrade continuously and maintain a consistently structured degradation interface formed of different layers made of Mg, $MgOH_2$, ACP, and CCP progressively evolving from the implant surface toward the natural bone. In short, degradation products formed at the Mg alloy interface results in CCP similar to the bone and get resorbed by the OC to induce bone formation by the OB. Such stable structure of Mg alloy is deemed to be most suitable for biodegradable material and it is one of the key reasons behind the success of clinical progression in this study.

Previously reported in vivo studies have shown severe bone softening during the initial stage of implantation caused by the formation of a fibrous membrane around the load-bearing implant, despite the favorable bone formation phenomena by biodegradation of Mg alloy (32). However, successful bone formation outcome with minimal bone softening, which eventually gets replaced by the bone completely, can be obtained by minimizing the initial loading as shown in our clinical results.

Even though very limited scope of fracture cases were selected for the clinical examinations, it was difficult to apply one definite criterion over various bones of the hand and wrist fractures. However, due to their similarity in size, shape, and bone-healing mechanism, one can assume that the bones in hand and wrist fracture undergo a similar bone-healing process. In all 53 cases, fracture reunion was achieved within ~4–6 wk, and range of motion of the hand measured 6 mo after surgery was restored to nearly the same extent compared with the contralateral hand. Observation of X-ray images show a temporary shading of implant surroundings due to hydrogen gas formation. After implantation, very limited amounts of hydrogen gas were observed around the head part of the Mg alloy screw, which disappeared by being absorbed into surrounding in ~2–4 wk after surgery. Formation of gas cavities at the implantation site due to degradation process of Mg have been reported in several studies (33, 34). From a clinical perspective, such gas cavity formation would be detrimental for bone- and wound-healing processes (34). However, a 1-y follow-up study of Mg-Y-Re-Zr alloy in rabbit showed no bone erosion due to gas cavities (33). In our clinical study, the X-ray images at the early stage of implantation have shown atypical shades of surrounding bones and possibly an absence of cancellous bone surrounding the implanted screw. Such area increased and the dark shades reached its maximum size at 2–3 mo; it was then gradually reduced to be barely visible at 6 mo postoperation and was completely gone, along with the implanted screw, after 12 mo. Results from our in vivo study using Villanueva stain have proved that atypically shaded areas were not yet fully mineralized and matured bones, and X-ray images of patients at 6 mo and 1 y have concurred with the findings from the in vivo animal study. The clinical follow-up was done by X-ray in this work, with the consequence that exact degradation progress could not be monitored. In future works, we envisage to use CT scan so to be able to quantitatively assess the degradation rate of the implant.

In conclusion, a complete bone healing from biodegradable implant shown in our 1-y follow-up of clinical trial could be explained by the continuous degradation of Mg alloy and formation of biomimicking calcification matrix (CCP) at the degradation interface, which initiate the bone formation process. Simultaneous bone formation at the Mg alloy–bone interface allows slow yet controlled degradation of Mg alloy implant that, within 1 y, gets completely replaced by the new bone. Therefore, findings from this study provide new detailed understanding of the mechanisms by which biodegradable Mg alloy degradation can promote the process of new bone formation in substitution to the degrading fixation device. Importantly, results from the clinical trial reported herein suggest that the use of biodegradable Mg-based devices can avoid the necessity of a second surgical procedure, thus greatly improving the quality of life of the patients and shifting the century-old paradigm for bone fixation devices.

Methods

Preparation of Preclinical Examination Through in Vivo Model. All in vivo studies performed for this study have been reviewed and approved by the Animal Care and Use Committee (IACUC no. 2013-14-158) of Asan Medical Center. Animal models for 8-wk (n = 10) and 16-wk (n = 10) experiments were as follows: 12-wk-old New Zealand White rabbits weighing 2.5~3.0 kg were purchased (OrientBio) a week before the surgical procedure for habituation at Asan Medical Center. Zoletil (10 mg/kg; Virbac SA) and xylazine (5 mg/kg; Bayer Korea) were mixed at 2:1 ratio and i.m. injected as anesthesia. Minimally invasive incisions were made on the right femoral condyle, and an electric drill was used to create a hole of 2 mm in diameter and 6 mm in depth. After cleaning the holes with 0.9% sterile saline, Mg-5wt%Ca-1wt%Zn

alloy cylinder specimens (Ø 2 × 6 mm) were implanted. Incision was sutured with 5-0 black silk. The same procedures were performed for the left femoral condyle but cylindrical rods (Ø 2 × 6 mm) made of Ti6Al4V were implanted instead as controls. Rabbits were administered to the postsurgical unit after the surgery and monitored according to in-house regulations. Both incision sites were sterilized daily with antiseptic, and cefazolin (20 mg/kg) and ketorolac (1 mg/kg) were injected i.m. daily for a week as antibiotic and anti-inflammatory therapy. Incisional wounds were healed completely 4 wk postoperation. Animal models for 26-wk experiments ($n = 5$) went through the same surgical procedures as the 8- and 16-wk models, but received implantation of Mg-5wt%Ca-1wt%Zn cylindrical specimens (Ø 2 × 6 mm) on both femoral condyles. Calcein (10 mg/kg; Sigma C-0875) was s.c. administered 1 wk and 2 d before euthanasia. X-ray images of implantation sites were obtained and 3 mL of KCl (150 mg/mL) were i.v. administered as euthanasia. Implanted samples were extracted and placed in 99.99% (vol/vol) ethanol (EtOH). EtOH was changed every 12 h for 3 d for fixation.

Histological Analysis. Histological slide preparations were carried out at the Ito Bone Histomorphometry Institute (Niigagta, Japan). Samples gathered from the animal models were placed in Villanueva bone stain solution for 4 d and dehydrated in sequence using EtOH according to the laboratory protocol (35). Dehydrated samples were embedded in methyl methacrylate resin for 20 d at 30~40 °C to create bone blocks. Vertical cross-sectional images of bone blocks were obtained using μCT (SkyScan 1172) and hard tissue cutter (crystal cutter/diamond wheel; Maruto Co.) was used to cut the bone blocks into 300-μm sections that matched the dimension/planes from μCT images. Hard tissue grinder (grinding machine) was used to reduce the sections to 100 μm and then hand-polished to obtain 20- to 30-μm-thick tissue slides. Obtained slides were analyzed by optical (visible light) and fluorescence microscopy (OLYMPUS BX-53).

SEM/EDX. After examination of Villanueva staining, the compositional analysis of the same specimen was performed by EDX using FIB/SEM (Quanta 3D; FEI). EDX line profile and mapping were performed at 800× magnification and 15 kV.

TEM/EDX. For the microstructural analysis by TEM, specimens were prepared using Focused Ion Beam (Nova 600-NanoLab; FEI); then, bright-field images, SAD patterns, and EDX analysis were acquired with Tecnai F20 (FEI) at 200 kV. Electron diffraction profiles were obtained from the SAD patterns using PASAD, a DigitalMicrograph plug-in.

Clinical Trial. Following the clinical trial approval from the Korea Food and Drug Administration (KFDA Clinical Trial Approval for Medical Device no. 362), open label interventional study of developed biodegradable Mg alloy screws were conducted at Ajou University Hospital for patients with hand fractures requiring internal fixation. Subjects were recruited by a campaign that used print, Web, and radio advertisements. Patients were first screened by telephone, and qualifying patients were referred to study sites for further evaluation. All of the patients involved in this study participated voluntarily, and informed consents were obtained. Subjects were chosen from the pool if aged 20 y or older and there was no history of chronic bone disease. Patients were excluded from the pool if he or she had a severe infection, a severe soft tissue injury, comminuted fractures, open fracture, major systemic diseases (cancer, systemic metabolic disease), kidney disease with a blood Cr level higher than 1.4, or a disease that could affect the bone-healing process. After the surgery, outpatient visit follow-up was performed at 1 wk, 2 wk, 1 mo, 2 mo, 3 mo, 6 mo, and 1 y. Validation of bone fusion was conducted after 6 mo, and the safety evaluation was constantly performed until the end of clinical trial process at 1 y. Splints were removed after 2–3 wk postoperation, and patients were allowed to perform everyday activities depending on progress of bone union for the next 2–3 mo. Patients were allowed perform professional activity, muscle-using leisure activity, and sports after 3 mo postoperation with confirmation of bone fusion. Along with bone fusion assessment at 6 mo, passive range of motion, total active motion, hand grip power, DASH scale, and VAS scale were also measured. DASH scale was calculated using 30-item questionnaire answered by the patient subjects comparing physical function and symptoms before and after the surgery. The pain VAS was completed using 0–10 scores.

ACKNOWLEDGMENTS. We thank Hendra Hermawan and Daniele Pezzoli for useful discussions, help, and guidance throughout the writing of the manuscript. Support for this work was provided by the Basic Science Research Program through the National Research Foundation of Korea (NRF) funded by Ministry of Education Grant 2009-0093814 (to J.-W.L.); NRF Grant 2012R1A2A1A01006546 funded by the Korean government; KIST TRC Project 2E25501 and Seoul R&BD program, Seoul Development Institute, Republic of Korea Grant SS100008; and NRF Grant NRF-2015R1A2A2A01007430 (to P.-R.C.) funded by the Korean government.

1. Voggenreiter G, et al. (2003) Immuno-inflammatory tissue reaction to stainless-steel and titanium plates used for internal fixation of long bones. *Biomaterials* 24(2):247–254.
2. Liu X, Chu PK, Ding C (2004) Surface modification of titanium, titanium alloys, and related materials for biomedical applications. *Mater Sci Eng Rep* 47(3):49–121.
3. Valiev R (2004) Nanostructuring of metals by severe plastic deformation for advanced properties. *Nat Mater* 3(8):511–516.
4. Hench LL (1980) Biomaterials. *Science* 208(4446):826–831.
5. Hanker JS, Giammara BL (1988) Biomaterials and biomedical devices. *Science* 242(4880): 885–892.
6. Staiger MP, Pietak AM, Huadmai J, Dias G (2006) Magnesium and its alloys as orthopedic biomaterials: A review. *Biomaterials* 27(9):1728–1734.
7. Li N, Zheng Y (2013) Novel magnesium alloys developed for biomedical application: A review. *JMST* 29(6):489–502.
8. Wu G, Ibrahim JM, Chu PK (2013) Surface design of biodegradable magnesium alloys—a review. *Surf Coat Tech* 233:2–12.
9. Chen Y, Xu Z, Smith C, Sankar J (2014) Recent advances on the development of magnesium alloys for biodegradable implants. *Acta Biomater* 10(11):4561–4573.
10. Zheng Y, Gu X, Witte F (2014) Biodegradable metals. *Mater Sci Eng Rep* 77:1–34.
11. Li Z, Gu X, Lou S, Zheng Y (2008) The development of binary Mg-Ca alloys for use as biodegradable materials within bone. *Biomaterials* 29(10):1329–1344.
12. Witte F, et al. (2005) In vivo corrosion of four magnesium alloys and the associated bone response. *Biomaterials* 26(17):3557–3563.
13. Remennik S, Bartsch I, Willbold E, Witte F, Shechtman D (2011) New, fast corroding high ductility Mg-Bi-Ca and Mg-Bi-Si alloys, with no clinically observable gas formation in bone implants. *Mater Sci Eng B* 176(20):1653–1659.
14. Hoppe A, Güldal NS, Boccaccini AR (2011) A review of the biological response to ionic dissolution products from bioactive glasses and glass-ceramics. *Biomaterials* 32(11):2757–2774.
15. Yoshizawa S, Brown A, Barchowsky A, Sfeir C (2014) Magnesium ion stimulation of bone marrow stromal cells enhances osteogenic activity, simulating the effect of magnesium alloy degradation. *Acta Biomater* 10(6):2834–2842.
16. Windhagen H, et al. (2013) Biodegradable magnesium-based screw clinically equivalent to titanium screw in hallux valgus surgery: Short term results of the first prospective, randomized, controlled clinical pilot study. *Biomed Eng Online* 12:62.
17. Cha PR, et al. (2013) Biodegradability engineering of biodegradable Mg alloys: Tailoring the electrochemical properties and microstructure of constituent phases. *Sci Rep* 3:2367.
18. Murni NS, Dambatta MS, Yeap SK, Froemming GRA, Hermawan H (2015) Cytotoxicity evaluation of biodegradable Zn-3Mg alloy toward normal human osteoblast cells. *Mater Sci Eng C* 49:560–566.
19. Willbold E, et al. (2015) Effect of the addition of low rare earth elements (lanthanum, neodymium, cerium) on the biodegradation and biocompatibility of magnesium. *Acta Biomater* 11:554–562.
20. Fujibayashi S, Neo M, Kim HM, Kokubo T, Nakamura T (2003) A comparative study between in vivo bone ingrowth and in vitro apatite formation on Na2O-CaO-SiO2 glasses. *Biomaterials* 24(8):1349–1356.
21. Yang L, Zhang E (2009) Biocorrosion behavior of magnesium alloy in different simulated fluids for biomedical application. *Mater Sci Eng C* 29(5):1691–1696.
22. Riggs BL, Parfitt AM (2005) Drugs used to treat osteoporosis: The critical need for a uniform nomenclature based on their action on bone remodeling. *J Bone Miner Res* 20(2):177–184.
23. Lindsay R, et al. (2006) A novel tetracycline labeling schedule for longitudinal evaluation of the short-term effects of anabolic therapy with a single iliac crest bone biopsy: Early actions of teriparatide. *J Bone Miner Res* 21(3):366–373.
24. Delmez JA, et al. (1986) Continuous ambulatory peritoneal dialysis and bone. *Kidney Int* 30(3):379–384.
25. Song Y, Shan D, Chen R, Zhang F, Han EH (2009) Biodegradable behaviors of AZ31 magnesium alloy in simulated body fluid. *Mater Sci Eng C* 29(3):1039–1045.
26. Zhang S, et al. (2010) Research on an Mg-Zn alloy as a degradable biomaterial. *Acta Biomater* 6(2):626–640.
27. Zumdahl SS, Zumdahl SA (2008) *Chemistry* (Heath and Co., Lexington, MA), 8th Ed.
28. Moreno EC, Kresak M, Zahradnik RT (1974) Fluoridated hydroxyapatite solubility and caries formation. *Nature* 247(5435):64–65.
29. Van Santen RA (1984) The Ostwald step rule. *J Phys Chem* 88(24):5768–5769.
30. Yang X, et al. (2011) Influence of magnesium ions and amino acids on the nucleation and growth of hydroxyapatite. *CrystEngComm* 13(4):1153–1158.
31. Ding H, Pan H, Xu X, Tang R (2014) Toward a detailed understanding of magnesium ions on hydroxyapatite crystallization inhibition. *Cryst Growth Des* 14(2):763–769.
32. Thormann U, et al. (2015) The biocompatibility of degradable magnesium interference screws: An experimental study with sheep. *BioMed Res Int* 2015:943603.
33. Waizy H, et al. (2014) In vivo study of a biodegradable orthopedic screw (MgYREZr-alloy) in a rabbit model for up to 12 months. *J Biomater Appl* 28(5):667–675.
34. Kuhlmann J, et al. (2013) Fast escape of hydrogen from gas cavities around corroding magnesium implants. *Acta Biomater* 9(10):8714–8721.
35. Li C, et al. (2001) Long-term effect of incadronate disodium (YM-175) on fracture healing of femoral shaft in growing rats. *J Bone Miner Res* 16(3):429–436.